Atmos. Meas. Tech., 6, 1359–1369, 2013
www.atmos-meas-tech.net/6/1359/2013/
doi:10.5194/amt-6-1359-2013

Atmospheric Measurement Techniques
Open Access

Ground-based integrated path coherent differential absorption lidar measurement of CO_2: foothill target return

S. Ishii[1], M. Koyama[2], P. Baron[1], H. Iwai[1], K. Mizutani[1], T. Itabe[1], A. Sato[3], and K. Asai[3]

[1]National Institute of Information and Communications Technology, 4-2-1 Nukuikitamachi, Kogenei, Tokyo 184-8795, Japan
[2]Tokyo Metropolitan University, 6-6 Asahigaoka, Hino, Tokyo 191-0065, Japan
[3]Tohoku Institute of Technology, 35-1 Yagiyamakasumi Taihaku, Sendai, Miyagi 982-8577, Japan

Correspondence to: S. Ishii (sishii@nict.go.jp)

Received: 14 November 2012 – Published in Atmos. Meas. Tech. Discuss.: 29 November 2012
Revised: 24 April 2013 – Accepted: 2 May 2013 – Published: 23 May 2013

Abstract. The National Institute of Information and Communications Technology (NICT) has made a great deal of effort to develop a coherent 2 µm differential absorption and wind lidar (Co2DiaWiL) for measuring CO_2 and wind speed. First, coherent Integrated Path Differential Absorption (IPDA) lidar experiments were conducted using the Co2DiaWiL and a foothill target (tree and ground surface) located about 7.12 km south of NICT on 11, 27, and 28 December 2010. The detection sensitivity of a 2 µm IPDA lidar was examined in detail using the CO_2 concentration measured by the foothill reflection. The precisions of CO_2 measurements for the foothill target and 900, 4500 and 27 000 shot pairs were 6.5, 2.8, and 1.2 %, respectively. The results indicated that a coherent IPDA lidar with a laser operating at a high pulse repetition frequency of a few tens of KHz is necessary for XCO_2 (column-averaged dry air mixing ratio of CO_2) measurement with a precision of 1–2 ppm in order to observe temporal and spatial variations in the CO_2. Statistical comparisons indicated that, although a small amount of in situ data and the fact that they were not co-located with the foothill target made comparison difficult, the CO_2 volume mixing ratio obtained by the Co2DiaWiL measurements for the foothill target and atmospheric returns was about −5 ppm lower than the 5 min running averages of the in situ sensor. Not only actual difference of sensing volume or the natural variability of CO_2 but also the fluctuations of temperature could cause this difference. The statistical results indicated that there were no biases between the foothill target and atmospheric return measurements. The 2 µm coherent IPDA lidar can detect the CO_2 volume mixing ratio change of 3 % in the 5 min signal integration. In order to detect the position of the foothill target, to measure a range with a high SNR (signal-to-noise ratio), and to reduce uncertainty due to the presence of aerosols and clouds, it is important to make a precise range measurement with a Q-switched laser and a range-gated receiver.

1 Introduction

Atmospheric carbon dioxide (CO_2) was roughly constant before the beginning of the Industrial Revolution in the mid-18th century. Population growth has resulted in an increase in the consumption of fossil fuels, and human activities led to an increase in CO_2 emission. Atmospheric CO_2 concentration has increased rapidly from 280 ppm to greater than 380 ppm since the Industrial Revolution (IPCC, 2007). Data obtained from analyses of Antarctic ice cores and atmospheric observations indicate a relationship between the increase in CO_2 concentration and atmospheric temperature (Etheriddge et al., 1996). Because of the presence of CO_2 sinks such as the oceans or terrestrial ecosystems, atmospheric CO_2 increases at only half the rate of anthropogenic CO_2 emissions; however, in nature, the spatial-scale from regional to continental and the temporal variations in the CO_2 sinks are not well understood due to limited observations (Le Quéré et al., 2009). Continuous monitoring of CO_2 on a global scale is important for understanding the carbon cycle and estimating the carbon flux. Highly accurate ground-based and airborne measurements provide valuable data sets of the global CO_2 growth rate, seasonal information, hemispheric gradients, and so on. However, a lack of observation extends over

a huge area. Ground-based and airborne measurements are not representative of the huge area to accurately infer carbon fluxes. Spaceborne measurements are a promising approach for globally measuring the temporal and spatial distribution of XCO_2 (column-averaged dry air mixing ratio of CO_2). Spaceborne XCO_2 measurement with a bias-free high precision of 1–2 ppm is necessary to improve our knowledge of the carbon cycle (NASA Science Definition and Planning Workshop Report: Active Sensing of CO_2 Emissions over Nights, Days, and Seasons, 2008). In 2009, the Greenhouse gas Observing SATellite (GOSAT) (Kuze et al., 2009), equipped with spaceborne passive sensors, was launched to continuously monitor the global total CO_2 column concentration. The Orbiting Carbon Observatory-2 (Crisp et al., 2004) and GOSAT-2 will be launched for the same purpose in the near future. However, a passive sensor is affected by the presence of aerosols and clouds which might cause some underestimate of CO_2 total column optical depth measurements. These underestimates may result in regional biases in CO_2 surface flux inversions.

An integrated path differential absorption (IPDA) lidar is one of the promising next-generation spaceborne sensors. The IPDA lidar uses a pulsed narrow-line width laser and a range-gated receiver. A Q-switched laser and range-gated receiver are helpful for distinguishing returns from the Earth's surface from other returns such as aerosols and clouds. The IPDA lidar can measure the total column-averaged mixing ratio of trace gas using return signals from the Earth's surface or from thick clouds. The IPDA lidar has the potential of providing high measurement accuracy (bias close to zero), high precision (within a few ppm), ranging capability, and high sensitivity for detecting aerosol and clouds. The 1.6 µm and 2 µm spectral regions are suitable for XCO_2 measurement from space. The sensitivity of spaceborne lidar XCO_2 measurement has been investigated (Menzies and Tratt, 2003; Ehret et al., 2008; Kawa et al., 2010). The NASA Langley Research Center (LaRC) and the Japan Aerospace Exploration Agency (JAXA) developed a 1.57 µm laser absorption spectrometer (LAS) with modulated continuous wave and direct detection (Browell et al., 2010; Sakaizawa et al., 2010). NASA Goddard Space Flight Center (Abshire et al., 2010) and Deutsches Zentrum für Luft- und Raumfahrt (German Aerospace Center) (Amediek et al., 2008) used a 1.57 µm pulse laser and direct detection. Simulated weighting functions of a CO_2 absorption cross section (Menzies and Tratt, 2003; Ehret et al., 2008) shows that, compared to the 1.57 µm spectral region, the 2.05 µm region is more sensitive to lower troposphere CO_2 distribution where the sinks and sources interact with the atmosphere. Various 2 µm lasers have been developed for spaceborne IPDA lidar CO_2 measurement (e.g., Yu et al., 2006; Sato et al., 2012). A 2.05 µm IPDA lidar is one of the most promising next-generation spaceborne sensors. The NASA Jet Propulsion Laboratory (JPL) (Spiers et al., 2011) is developing a 2.05 µm LAS with a continuous wave laser and heterodyne detection. NASA LaRC (Koch et al., 2004, 2008), the Institute Pierre Simon Laplace École Polytechnique (Gibert et al., 2006, 2008), and the National Institute of Information and Communications Technology (NICT) (Ishii et al., 2010, 2012) reported 2.05 µm DIfferential Absorption Lidar (DIAL) by using a pulse laser, heterodyne detection, and aerosols and clouds (atmospheric return). We evaluated the performance of horizontal and vertical CO_2 measurements using aerosol and cloud returns (Ishii et al., 2010, 2012). In this paper we describe the horizontal CO_2 measurement using a foothill target. In the next section, we briefly describe our coherent 2 µm differential absorption and wind lidar (Co2DiaWiL) and discuss the retrieval method of CO_2 and the error analysis in Sect. 3. We explain the measurement strategy and experimental setup in Sect. 4. In Sect. 5, we describe the detection sensitivity of the IPDA lidar using experimental long-range CO_2 measurements, the statistical results of CO_2 measurements, and the comparison with the ground-based in situ measurements.

2 Coherent 2 µm differential absorption and wind lidar

The Co2DiaWiL specifications are listed in Table 1. Since the Co2DiaWiL is described in detail in our previous work (Ishii et al., 2012), we present its main characteristics. The Co2DiaWiL has a single-frequency Q-switched Tm,Ho:YLF laser with laser frequency offset locking technique, a 10 cm-aperture Mersenne off-axis telescope, a two-axis scanning device, two heterodyne detectors, and signal processing devices. The single-frequency Q-switched Tm,Ho:YLF laser with a 2.05 µm operating wavelength demonstrates 80 mJ output energy with a 150 ns pulse width (full width at half maximum (FWHM)) at a 30 Hz pulse repetition frequency. The Co2DiaWiL uses two wavelengths referred to as on- and off-line lasers for measuring CO_2 concentration. The two laser wavelengths are selected. The wavelength of the on-line laser corresponds to the center or wing of the absorption line of the target molecule, while the wavelength of the off-line laser lies in the far wing of the absorption line. We use the R30 absorption line of the $(20^\circ 1)_{\mathrm{III}} \leftarrow (00^\circ 0)$ band of CO_2. The wavelength of the on-line laser can be set within the range of 2051.002–2051.058 nm using laser frequency offset locking. Based on the signal-to-noise ratio, we set the wavelength of the on-line laser at 2051.058 nm in order to conduct long-range CO_2 measurements. The wavelength of the off-line laser was set at 2051.250 nm. The absolute frequency stability of the injected pulsed laser is dominated by mechanical fluctuations of the piezoelectric transducer (PZT) that controls resonator length. The absolute frequency stability of the injected pulsed laser is 1 MHz at most, which is sufficient for CO_2 measurement with a high precision. The off-line laser is controlled only by adjusting the resonator temperature and piezoelectric movement of the output coupler element. The wavelength drift of the off-line laser is smaller than 7 pm, which corresponds to a maximum

change of 0.04 % in the on–off difference absorption cross section. The interferences due to the presence of other atmospheric gases except for the water vapor are almost negligible. The absorption due to water vapor (relative humidity = 10 to 70 %) could bring an error of 0.1 to < 0.3 % in the CO_2 volume mixing ratio derived from the IPDA lidar measurement. The on- and off-line laser pulses are alternately switched every 1 shot. The pulsed laser beam is emitted into the atmosphere by using a 10 cm off-axis telescope and a waterproof 2-axis scanning device. The signal backscattered by moving aerosol particles or reflected by a foothill target is detected using the heterodyne technique on an InGaAs-PIN photodiode. The heterodyne detection is operated under shot-noise-limited condition of about 9 dB. A small portion of the pulsed laser beam is also detected using the heterodyne technique to monitor the frequency and lasing time of the outgoing laser pulse on a balanced InGaAs-PIN photodiode. The outputs of these detectors are digitized at 500 MHz by using 8-bit analog-to-digital (AD) converters. The power spectra of the outgoing on- and off-line laser pulses and backscattered signals were obtained by 4096- and 512-point fast Fourier transform (FFT), respectively. The power spectra of on- and off-line backscattered signals were obtained using an algorithm proposed by Frehlich et al. (1997). Data related to laser pulses with a frequency difference of more than 1.25 MHz from the average intermediate frequency (i.e., 105 MHz) were discarded. The ratio of discarded laser shot pairs was only around 5 % in the emitted laser shot pairs.

Table 1. Specifications of coherent 2 µm differential absorption and Doppler wind lidar.

Transmitter	
Laser	Tm,Ho;YLF
Wavelength	2051.058 nm (On)/2051.250 nm (Off)
Pulse energy	50–80 mJ/pulse (Operational)
Pulse width (FWHM)	150 ns
Pulse repetition	30 Hz
Polarization	Circular
Receiver	
Telescope type	Mersenne off-axis
Diameter	0.1 m
Magnification	10
Detector for reference signal	Balanced InGaAs-PIN photodiode
Detector for backscattered signal	InGaAs-PIN photodiode
Scanner	
Scanning range	Azimuth −10° to 370° Elevation −20° to 200°
Effective clear aperture	0.1 m
Scanning resolution	0.01°
Scanning speed	up to 60° s^{-1}
Signal processing	
Signal sampling frequency	500 MHz
Resolution	8 bits
FFT-point (reference)	4096
FFT-point (signal)	512
Range resolution	150 m

3 Estimation of CO_2 and error analysis

The power $P_{i=\mathrm{On,Off}}(R)$ of backscattered signals from the foothill target and atmosphere can be expressed as

$$P_i(R) = \frac{\xi_i \cdot P_{0,i} \cdot A \cdot \rho}{\pi \cdot R^2} \cdot \exp(-2 \cdot \int_0^R \alpha_i(r)\,\mathrm{d}r), \quad (1)$$

(foothill target)

$$P_i(R) = \frac{\xi_i \cdot P_{0,i} \cdot A \cdot \beta(R) \cdot c \cdot \tau_p/2}{R^2} \cdot \exp(-2 \cdot \int_0^R \alpha_i(r)\,\mathrm{d}r), \quad (2)$$

(atmosphere)

where R (m) is the range, ξ_i is the total instrument efficiency for the wavelength i, $P_{0,i}$ is the laser output power, A (m^2) is the receiver area, ρ is the surface reflectance, where we assume that the foothill target is Lambertian, $\alpha_i(r)$ (m^{-1}) is the extinction coefficient of the atmosphere, $\alpha_i(r)$ is defined as $\alpha_i(r) = \alpha_{\mathrm{atm}}(r) + \sigma_i(r)\rho_{\mathrm{CO_2}} N_{\mathrm{air}}$, where $\sigma_i(r)$ (m^{-2}) is the absorption cross section of CO_2, $\rho_{\mathrm{CO_2}}$ is the dry air volume mixing ratio of CO_2, N_{air} (m^{-3}) is the dry air number density, $\alpha_{\mathrm{atm}}(r)$ (m^{-1}) is the extinction coefficient associated with any other extinction processes, $\beta(R)$ ($m^{-1}\,sr^{-1}$) is the backscattering coefficient of the atmosphere, c ($m\,s^{-1}$) is the light velocity and $\tau_p(s)$ is the laser pulse duration. Since the on- and off-line wavelengths are sufficiently close, we can neglect the wavelength dependence of instrument efficiency, surface reflectance, and extinction coefficient except for CO_2 absorption.

The carrier-to-noise ratio CNR_i is defined as

$$\mathrm{CNR}_i = \frac{\langle P_i(R) \rangle}{\langle P_{i,N} \rangle}, \quad (3)$$

where $\langle P_i(R) \rangle$ and $\langle P_{i,N} \rangle$ are the mean power of the backscattered signal and the mean noise power. The theoretical signal-to-noise ratio $\mathrm{SNR}_i(R)$ for the squarer estimator described by Rye and Hardesty (1997) is given as

$$\mathrm{SNR}_i(R) = \sqrt{N_{\mathrm{L}} \cdot N_{\mathrm{C}}} \cdot \frac{\mathrm{CNR}_i}{1 + \mathrm{CNR}_i}, \quad (4)$$

where N_{C} is the number of coherent cells, and N_{L} is the number of on- and off-line laser shots. In this paper, N_{C} for the atmospheric return signal is calculated using Eq. (4) described by Gibert et al. (2006), and for the foothill target it is calculated using Eq. (6.1-29) obtained from Goodman (2000).

By applying Eqs. (1) and (2) to ranges R_1 and R_2 and to the on- and off-line wavelengths, absorption cross sections $\sigma_i(r)$ (m^{-2}) and the dry air number density N_{air} (m^{-3}), the differential absorption optical depth (DAOD) due to CO_2 absorption in the range between R_1 and R_2 can be obtained as follows:

$$\mathrm{DAOD} = \int_{R_1}^{R_2} \rho_{\mathrm{CO_2}}(r) \cdot N_{\mathrm{air}}(r) \cdot \{\sigma_{\mathrm{On}}(r) - \sigma_{\mathrm{Off}}(r)\}\,\mathrm{d}r$$
$$= \frac{1}{2} \cdot \log\left(\frac{P_{\mathrm{On}}(R_1) \cdot P_{\mathrm{Off}}(R_2)}{P_{\mathrm{Off}}(R_1) \cdot P_{\mathrm{On}}(R_2)}\right). \quad (5)$$

The dry air volume mixing ratio of CO_2 is obtained by assuming that ρ_{CO_2} and meteorological elements do not change between R_1 and R_2.

$$\rho_{\mathrm{CO_2}} = \frac{1}{2 \cdot N_{\mathrm{air}} \cdot \sigma \cdot (R_1 - R_2)} \cdot \left(\mathrm{DAOD} - \mathrm{DAOD}_{\mathrm{H_2O}}\right), \quad (6)$$

$$N_{\mathrm{air}} = \frac{P}{k \cdot T} \cdot \frac{1}{1 + \rho_{\mathrm{H_2O}}}, \quad (7)$$

where $\sigma (= \sigma_{\mathrm{On}} - \sigma_{\mathrm{Off}})$ is the difference between the absorption cross sections corresponding to the wavelengths of the on- and off-line lasers, P is pressure, T is temperature, k is the Boltzmann constant, ρ_{H_2O} is the water vapor (H_2O) volume mixing ratio, and DAOD_{H_2O} is the DAOD due to the H_2O absorption between R_1 and R_2. The difference between the absorption cross sections σ depends on both pressure and temperature.

The relative error ΔDAOD/DAOD between 0 and R is given by

$$\frac{\Delta\mathrm{DAOD}(0,R)}{\mathrm{DAOD}(0,R)} \cong \frac{1}{2 \cdot \mathrm{DAOD}(0,R)} \sqrt{\frac{1}{\mathrm{SNR}^2_{\mathrm{On}}(R)} + \frac{1}{\mathrm{SNR}^2_{\mathrm{Off}}(R)}}. \quad (8)$$

The experimental $\mathrm{SNR}_i(R)$ is $\langle P_i(R)\rangle / \Delta(\langle P_i(R)\rangle)$. $\Delta(\langle P_i(R)\rangle)$ is the standard deviation of $\langle P_i(R)\rangle$. The temporal cross-correlation coefficient between $P_{\mathrm{On}}(R)$ and $P_{\mathrm{Off}}(R)$ is required to estimate the ΔDAOD/DAOD. In this paper we assume the temporal cross-correlation coefficient as 0 to avoid the practical difficulties. The temporal cross-correlation coefficient for the foothill target return would be different from that for atmospheric return. The difference might have an impact on the precision of the IPDA lidar measurement comparing to the DIAL measurement. The relative error $\Delta\mathrm{DAOD}(R_1, R_2)$/DAOD (R_1, R_2) between R_1 and R_2 can be expressed as

$$\frac{\Delta\mathrm{DAOD}(R_1,R_2)}{\mathrm{DAOD}(R_1,R_2)} \cong \frac{1}{2 \cdot \mathrm{DAOD}(R_1,R_2)} \sqrt{\frac{1}{\mathrm{SNR}^2_{\mathrm{On}}(R_1)} + \frac{1}{\mathrm{SNR}^2_{\mathrm{Off}}(R_1)} + \frac{1}{\mathrm{SNR}^2_{\mathrm{On}}(R_2)} + \frac{1}{\mathrm{SNR}^2_{\mathrm{Off}}(R_2)}}. \quad (9)$$

The relative error $\Delta\rho_{CO_2}/\rho_{CO_2}$ is obtained using Eq. (10), DAOD, and meteorological data as follows:

$$\frac{\Delta\rho_{\mathrm{CO_2}}}{\rho_{\mathrm{CO_2}}} = \sqrt{\left(\frac{\Delta N_{\mathrm{Air}}}{N_{\mathrm{Air}}}\right)^2 + \left(\frac{\Delta\sigma}{\sigma}\right)^2 + \left(\frac{\Delta\mathrm{DAOD}}{\mathrm{DAOD}}\right)^2}. \quad (10)$$

To compare with the results of the foothill target return, the CO_2 volume mixing ratio was also calculated using atmospheric returns and the slope method (Gibert et al., 2006) under assumptions that the CO_2 volume mixing ratio and CO_2 absorption cross sections do not change between R_1 and R_2.

4 Ground-based in situ measurements

Pressure, temperature, relative humidity, wind speed, and wind direction were measured using an automatic weather station (Vaisala WXT510) set up on the roof of a four-story building at NICT (a section of the building has five stories). The average values of the meteorological data for each 1 min interval were automatically stored in a computer. The accuracies of pressure, temperature, and relative humidity are better than ± 0.5 hPa, $\pm 0.3\,^{\circ}$C and $\pm 3\,\%$, which lead to a total error of 0.1 % in the CO_2 volume mixing ratio on the IPDA lidar measurement. The total error of 0.1 % is for the atmosphere near the NICT building. However, the f1uctuations of temperature might have been larger than 1 °C due to the heterogeneous radiative properties of the surface over the 7 km measurement pass. For instance the temperature difference between within and above the canopy is about 1 °C in an urban area of Tokyo (Kanda et al., 2005), which corresponds to an error of 0.5 %. Thus, although the R30 absorption line of CO_2 is rather insensitive to temperature, the f1uctuations of temperature along the 7 km measurement path result in additional uncertainty. Spectroscopic errors also include error on the parameter values (pressure broadening and line strength). Additional measurements of CO_2 and H_2O concentrations were carried out at 1 min intervals with an in situ sensor (LI-COR Model LI-840, non-dispersive infrared CO_2/H_2O gas analyzer). The in situ sensor was installed in an observation room on the fifth-floor roof of the same building at NICT. Air entered the sensor at a flow rate of 1 L min^{-1} through an inlet located approximately 2 m above the roof. The inlet for the in situ sensor was about 4 m higher than the automatic weather station. Calibrations were made before measurements with 0, 358, and 452 ppm CO_2 standard reference gases. The accuracy of the analyzer was better than 1.5 %, and the root-mean-square value of the measured fluctuation was less than 1 ppm for a CO_2 volume mixing ratio of 370 ppm and for 1 s filtering. In situ measurement was recorded after 1 min integration. The measured CO_2 data were compared with the results obtained from DIAL measurements.

5 Experimental foothill target measurement

Figure 1a and b show the detailed topography and cross section around the target area. The laser beam was directed horizontally southward by using the 2-axis scanning device from NICT. It propagated 20 to 40 m above the surface and went through a commercial area, highway, and the Tama River before it hit the target surface. The foothill target is

located approximately 7 km south of NICT. Figure 2a shows an example of the outgoing off-line laser pulse signal (gray line) and the off-line return signal (black line) obtained using 500 MHz-sampling-rate, 8-bit AD converters. Arrows a and b indicate the peak time of lasing with Q-switching and the signal from the foothill target. Figure 2b shows the square of the intermediate-frequency (IF) signals of the outgoing off-line laser pulse. Figure 2c through e show the square of the intermediate-frequency signals of the off-line return signal for 9th, 1051th, and 3874th laser shot. We define the range between the Co2DiaWiL and the foothill target as the time difference at the two peaks. We can see from Fig. 2c through e that the peak moved back and forth. Figure 3a and b show examples of the range between the Co2DiaWiL and the foothill target measured using the on- and off-line lasers from 01:50 to 01:55 JST (Japan Standard Time) on 11 December 2010. The range fluctuations shown in Fig. 3a and b were induced mainly by speckle-induced intensity fluctuation. We also believe that unstable pointing (e.g., swaying branches) of the laser beam at the foothill target might have caused range fluctuations. The average ranges for the on- and off-line lasers for 1 min intervals were 7.089 (±0.010)–7.091 (±0.011) and 7.091 (±0.012)–7.093 (±0.012) km, and the average ranges for 5 min intervals were 7.090 (±0.011) and 7.092 (±0.012) km. The pulse width of 150 ns corresponds to the range resolution of 0.023 km. Uncertainties of ±0.012 km were expected. The frequency distributions of the measured range for the on- and off-line lasers were constructed and are shown in Fig. 3c. This figure also shows that the measured range was distributed widely between 7.08 and 7.11 km. Figure 3c indicates two different modes in the detection of the foothill target return. The slope angle was assumed to be about 12° from the topographic data around the target area. If there were 5 m-height trees around the target area and if the laser beam would pass through the trees, the length from the tree to the ground surface would correspond to be about 23.5 m (= 5 m/tan 12°). The two different modes suggest that the foothill target returns are a mix of trees and ground surface reflection. We used the range resolution of 150 m for determining a correct range to ignore uncertainties of ±0.012 km due to effects of the speckle-induced intensity fluctuation and to the two different modes. The foothill target was included at a range of 7.12 (±0.075) km.

Figure 4 shows the CNR_i's for the on-line (gray line) and off-line (black line) laser pulses obtained from the foothill target and atmospheric returns. The CNR_i was calculated using the power spectra of the backscattered signals. The CNR_i's of the on- and off-line laser decreased slowly with increasing range up to 6.97 km, and a CNR_i higher than 30 dB was observed at a range of 7.12 km. The foothill target return was much stronger than the atmospheric return. Though the power at the range of 7.12 km may include the contribution from the atmospheric return, it is 0.1 % of the power of the foothill target at most and negligible for the estimation of the XCO_2.

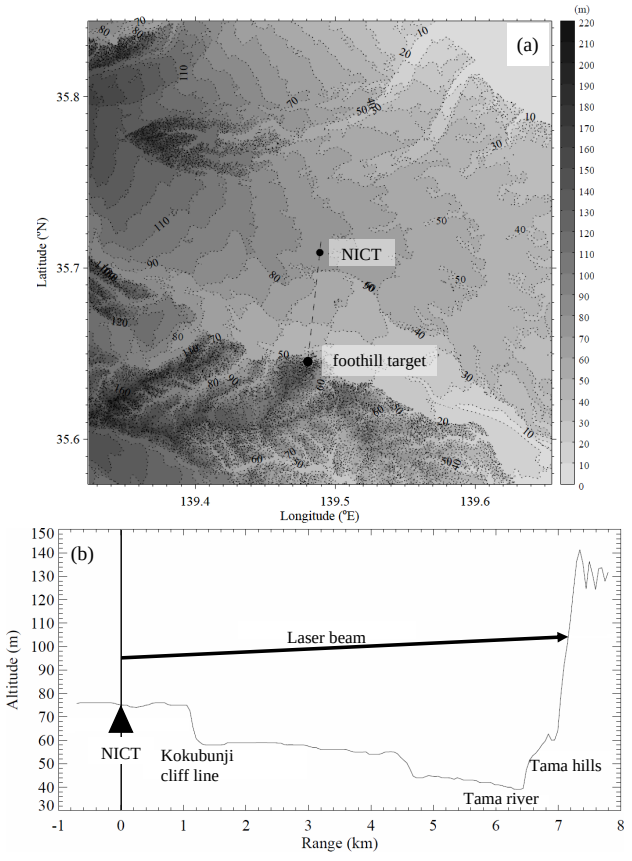

Fig. 1. (a) Map of area around NICT, foothill target, and investigated areas. Contour lines are represented at intervals of 10 m. **(b)** Cross section of topography data from NICT towards foothill target.

The relation between the range and DAOD ($R_1 =$ 0.974 km) for various shot pairs are shown in Fig. 5a. The DAOD for the 900 and 4500 shot pairs showed large fluctuations for distances greater than 4 km due to the decrease in the CNR_i, while for the 27 000 shot pairs, no large fluctuations were found. Figure 5a shows negative optical depths for the three shot pair cases at a range of 0 km, which raises the issue of calibration of absolute measurement of optical depth. The calibration is necessary to obtain an accurate optical depth with the IPDA lidar measurement. Gibert et al. (2008) suggested that the bias of the optical depth is negligible for high SNRs of on- and off-line backscattered signals. In this paper, the calibration was carried out at a range of 0.974 km. The optical depths are computed with respect to the position. The bias of the optical depth was calculated using Eq. (C5) described by Gibert et al. (2008). The SNRs of on- and off-line backscattered signals for the 900 shot pair were > 40 at ranges of 0.974 and 7.12 km. The calculated bias of the optical depth was -5.2×10^{-7}. The low bias of the optical depth does not affect the measurement of optical depth in our IPDA lidar experiments. Figure 5b shows the relation between the

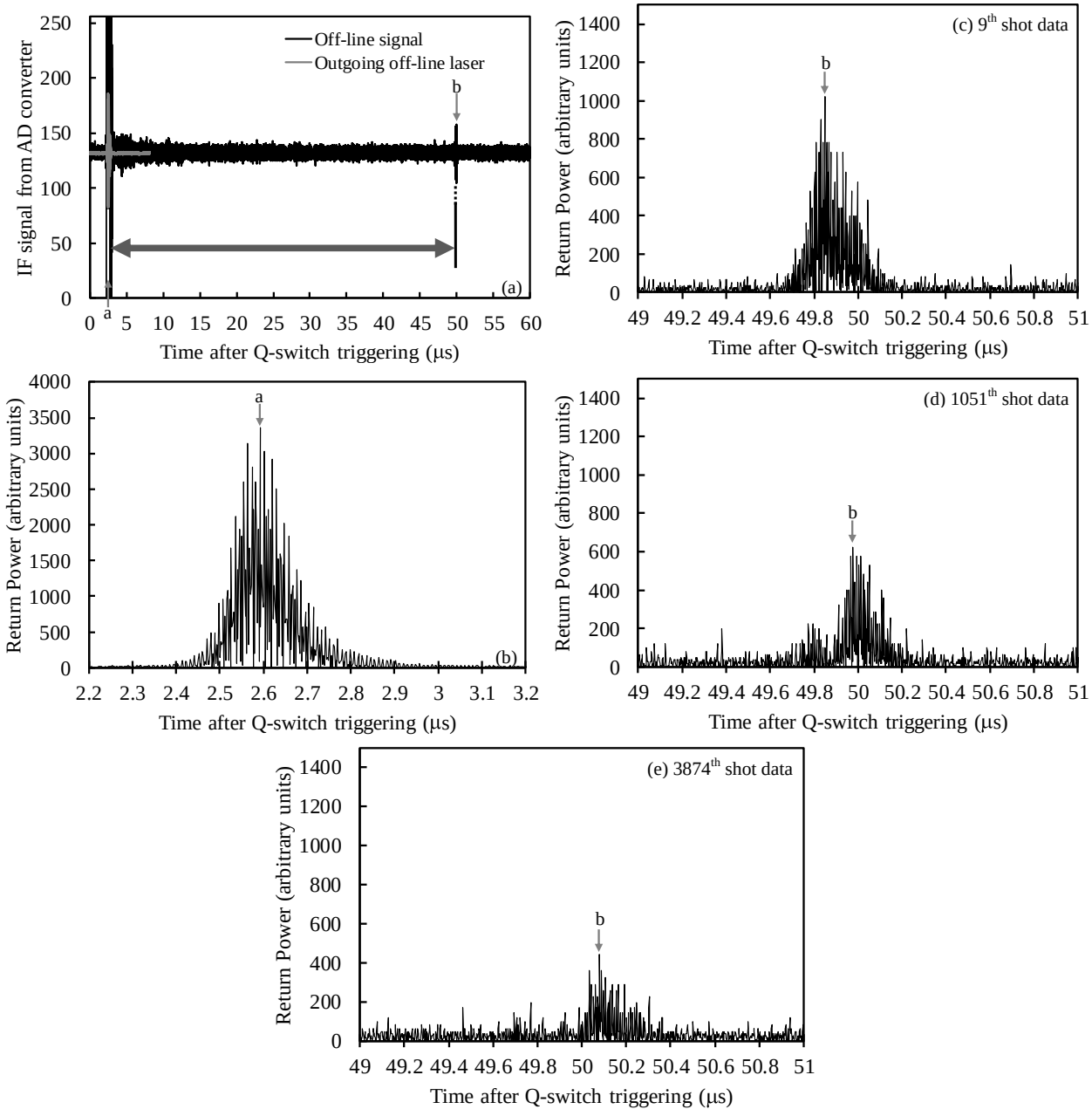

Fig. 2. (a) Outgoing laser pulse and atmospheric return signals versus time recorded using 8-bit AD converters. **(b)** A-scope display of outgoing laser pulse. A-scope display of foothill target return signal for **(c)** 9th **(d)** 1051th, and **(e)** 3874th laser shots. Labels "a" and "b" show peak location for outgoing laser pulse and foothill target return signal.

range and relative error of the DAOD for the three shot pair cases. The minimum relative errors of the DAOD for the three laser shot pairs in the range of 1 to 7 km were 13, 5.8, and 2.7 %, respectively. The relative error at short ranges was large due to the small DAOD and low heterodyne efficiency. The heterodyne detection measurement was also limited by speckle-induced fluctuation. The relative error of the DAOD at the range of 7.12 km was about two times lower than the minimum relative errors at the range between 1 and 7 km. The relative errors of the DAOD for the three laser shot pairs at the foothill target bin were 6.5, 2.8, and 1.2 %, respectively.

The probability density functions (PDFs) of on- and off-line backscattered power follows a gamma density function and N_C is equal to the normalized variance of the backscattered power, which is calculated using Eq. (6.1-29) described by Goodman (2000). The PDFs for on- and off-line normalized power for the 27 000 shot pair measured from 01:50 to

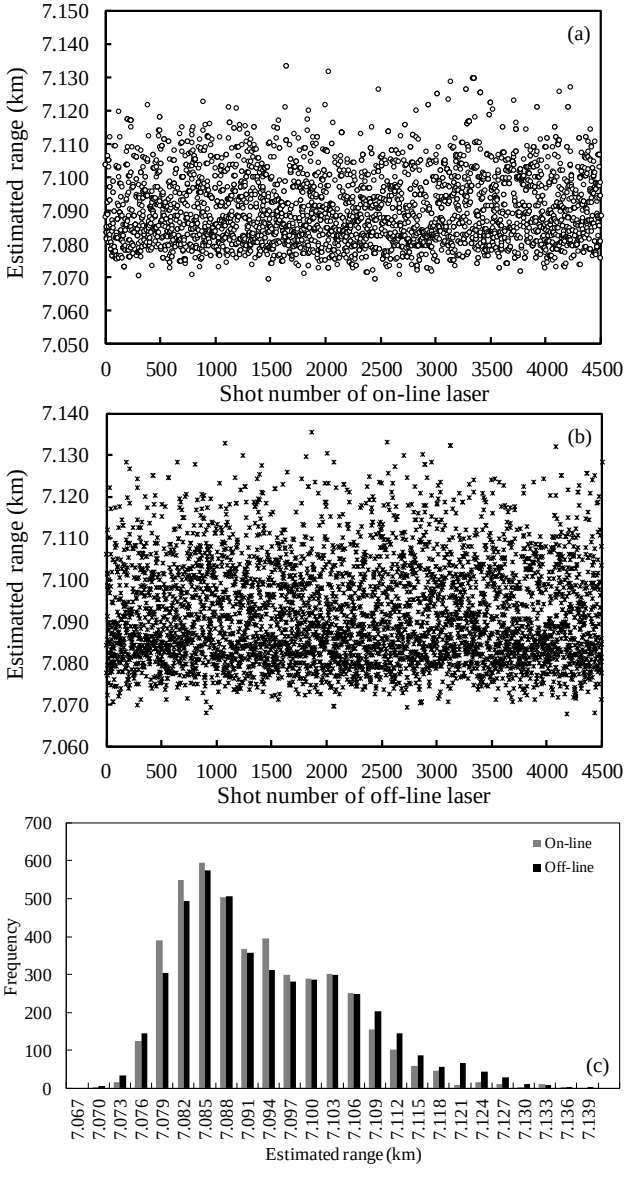

Fig. 3. Range estimated from time difference between labels "a" and "b" in Fig. 2a for **(a)** on-line laser pulse and **(b)** off-line laser pulse and **(c)** frequency of estimated range for on- and off-line laser pulse. Measurements were conducted from 01:50 to 01:55 JST on 11 December 2010.

02:20 JST on 11 December 2010 are shown in Fig. 6. The PDF follows a gamma density function with $N_C = 1.9$ calculated using Eq. (6.1-29). If signals were backscattered only by ground surface, we could expect to have a PDF in negative exponential function. The result suggests that the Nc of 1.9 was obtained due to the characteristics of mix target of trees and ground surface. The PDF shape is better represented by a gamma function. The calculated N_C for the atmospheric return amounts to 10.1 using a pulse width of 150 ns and a range gate duration of 1000 ns, and Eq. (4) described by Gibert et al. (2006). The experimental value of

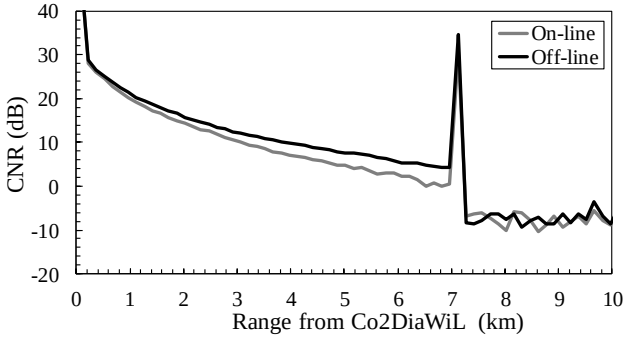

Fig. 4. Carrier-to-noise ratio (CNRi) for on- and off-line laser pulses. Measurements are same as those in Fig. 3. Peaks at 7.1 km show the CNR of foothill target return.

N_C for the atmospheric return was 9 to 10. In the present experiment we cannot say anything about the effects of the turbulence, although the Nc for atmospheric return depends not only on the pulse width but also on the turbulence in the atmosphere. The improvement of the signal-to-noise ratio for the coherent IPDA lidar due to Nc is limited if the Nc is small. Figure 7 shows the relation between the average number of pulses and relative error of the DAOD for various shot pairs. We compared the theoretical and experimental values of the relative error of the DAOD. The theoretical values were calculated using Eqs. (4) and (9), and the results are shown as a black solid line in Fig. 7. The relative error of the DAOD by signal segmental averaging was found to decrease as $N_L^{-1/2}$. Increasing the number of shot pairs in our experimental measurement will decrease the relative random error. The coherent IPDA lidar with the laser at a pulse repetition frequency of a few tens of KHz is necessary in order to reach the goal of 1–2 ppm relative error with a horizontal resolution of 100 km × 100 km for spaceborne observation (Ehret et al., 2008; NASA Science Definition and Planning Workshop Report, 2008).

The horizontal experimental CO_2 measurements were done continuously from 12:10 JST on 27 December to 16:02 JST on 28 December 2010. The temporal variations of the CO_2 volume mixing ratio measured using the Co2DiaWiL and the in situ sensor are shown in Fig. 8a and b. The closed and open circles show results obtained from the foothill target and atmospheric returns, respectively. The gray line shows the data obtained from the in situ sensor. The time-series of N_C's for on- and off-line backscattered power is shown in Fig. 8c. The data show that the N_C's for on- and off-line backscattered power were 1.5–1.9 during the day and 1.7–2.2 during the night. The N_C's were roughly constant during the experimental period. The 4500 shot pairs were used to estimate the CO_2 volume mixing ratios for both foothill target and atmospheric returns. The CO_2 volume mixing ratio for the foothill target return was obtained with a DAOD (Eq. 5) between 0.974 and 7.12 km and Eq. (6).

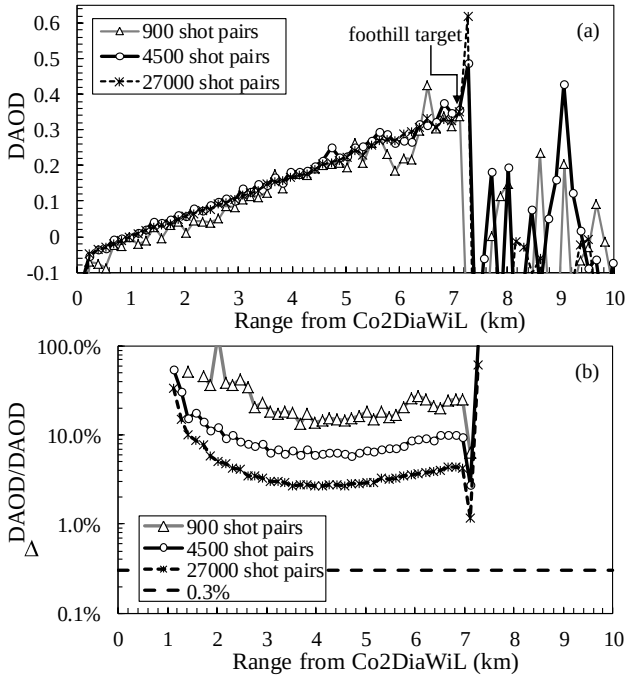

Fig. 5. Relation between range and **(a)** differential absorption optical depth (DAOD) and **(b)** relative error of DAOD for 900 (open triangle), 4500 (open circle), and 27 000 (asterisk) shot pairs. Measurements were conducted from 01:50 to 02:20 JST on 11 December 2010. Dashed line shows relative error of DAOD of 0.3 % corresponding to 1 ppm in CO_2 volume mixing ratio.

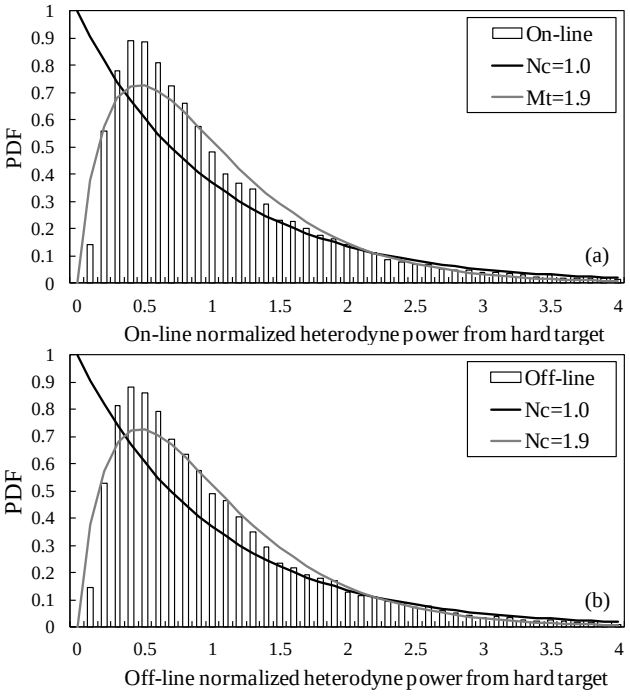

Fig. 6. Histogram of PDFs for **(a)** on-line and **(b)** off-line normalized heterodyne power for 27 000 returns from the 7.12 km-distant foothill target. Measurements are same as those in Fig. 5. PDF follows a gamma function with Nc = 1.9, plotted as gray solid line. Solid line is a negative exponential distribution.

The CO_2 volume mixing ratio for the atmospheric return was estimated from a slope of 40 range-gated bins for a range between 0.974 and 6.97 km. The distribution of CO_2 volume mixing ratio can be measured by using the slope method. The CO_2 volume mixing ratio change of 3 % is detectable by 5 min (or 4500 shot pairs) measurements in both methods. Though a more localized plume can be detectable in the DIAL measurement with atmospheric return, IPDA results are more stable. We compared the detection sensitivity of the IPDA lidar measurement with that of the DIAL measurement, in which the CO_2 volume mixing ratio for the atmospheric return was estimated by using the slope method. The precision values of the Co2DiaWiL measurements for the foothill target and atmospheric returns shown in Fig. 8a and b were in the range of 2.8–5.3 and 1.5–11.0 %. Although meteorological data were not obtained close to the target surface, the data measured using our automatic weather station were used to calculate the absorption cross section of CO_2 for the on- and off-line lasers. Since the difference between the pressure measured using our automatic weather station and that at the foothill target was smaller than 1 hPa, the pressure induced error on the retrieved CO_2 volume mixing ratio was negligible. However, if the temperature difference between the two points were larger than 1 °C, it would result in a difference larger than 0.5 % in the CO_2 volume

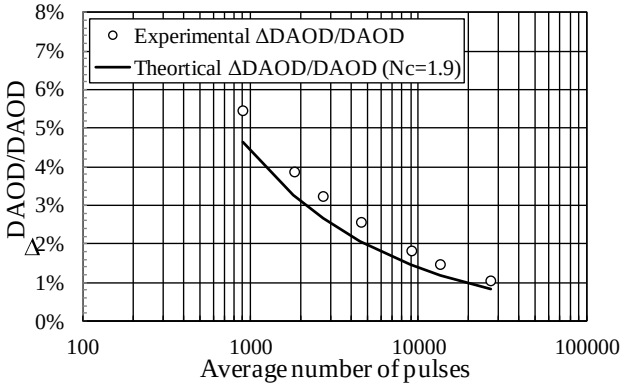

Fig. 7. Calculated relative error of DAOD for various shot pairs. Measurements are same as those in Fig. 5.

mixing ratio. The error due to the on–off difference absorption cross section was 0.07 % in the CO_2 volume mixing ratio on the Co2DiaWiL measurement. The frequencies of differences between the Co2DiaWiL measurements for the foothill target and atmospheric returns and the 5 min running averages of the in situ sensor are shown in Fig. 9. The CO_2 volume mixing ratio estimated from the foothill target and atmospheric returns shows that the Co2DiaWiL CO_2 measurements are not always lower/higher than the in situ sensor

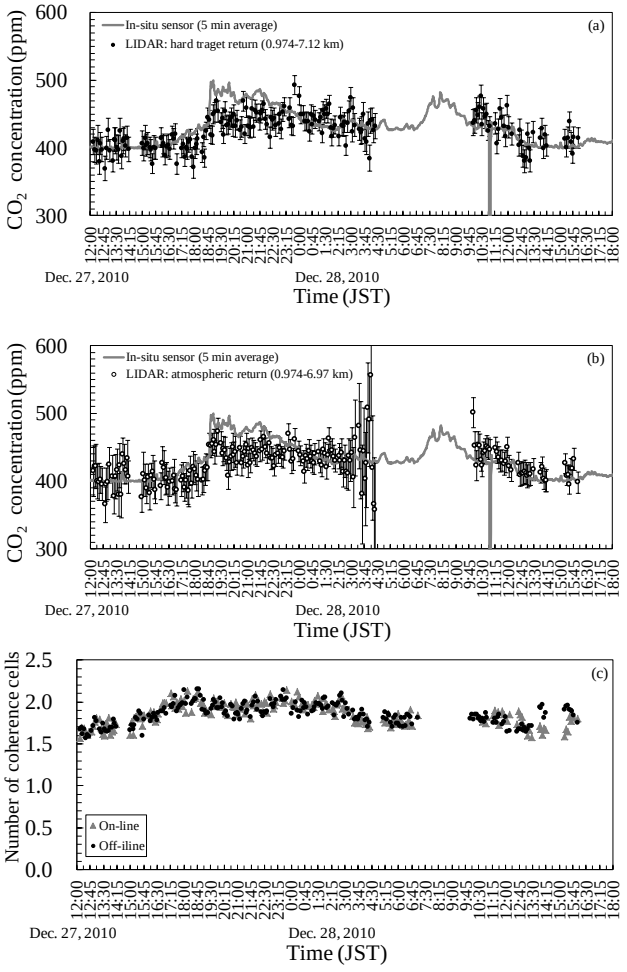

Fig. 8. Temporal variations of CO_2 concentrations measured using Co2DiaWiL and in situ sensor on 27 and 28 December 2010: **(a)** foothill target return and **(b)** atmospheric return. Laser frequency offset was 6.5 GHz for horizontal CO_2 measurement. **(c)** Time-series of Nc: (△) on- and (●) off-line laser pulse.

measurements. These measurements for the foothill target and atmospheric returns showed −4.6 and −5.0 ppm lower mean values than the 5 min running averages of the in situ sensor. The difference of 5 ppm might be interpreted as a bias. The root-mean-square of the absolute values of difference between the Co2DiaWiL measurements for the foothill target and atmospheric returns and the 5 min running averages of the in situ sensor were 26.1 and 25.9 ppm. These statistical results indicate that the root-mean-square of the absolute values of the difference of the foothill target return measurement was almost the same as that of the atmospheric return measurement. The causes of the differences between the Co2DiaWiL and the in situ sensor are sampling volume, sampling location, and sampling height. It should also be emphasized that these results were just an isolated comparison. Figure 10 shows the precision frequencies of the Co2DiaWiL measurements for the foothill target and atmospheric returns

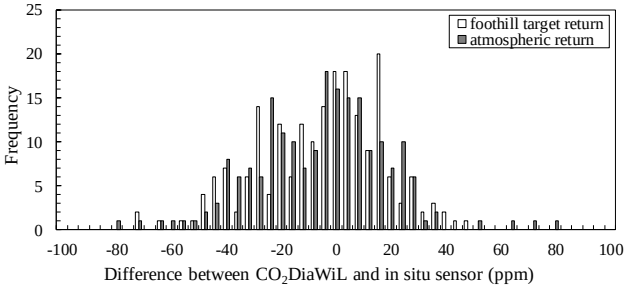

Fig. 9. Frequency of differences between Co2DiaWiL measurement and 5 min running mean of in situ sensor.

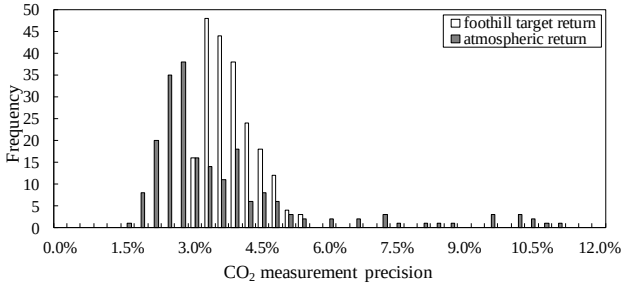

Fig. 10. Frequency of Co2DiaWiL measurement precision for foothill target and atmospheric return.

conducted on December 27 and 28. The precisions of the foothill target return measurement were mostly less than 3.8 %. On the other hand, the high-precision frequencies of the atmospheric return measurement were less than approximately 3.3 %. It should be noted that, although the long-range DIAL CO_2 measurement with the atmospheric return can result in highly precise measurement, precision depends strongly on the backscattering coefficient of the atmosphere and the atmospheric condition. An important point is that the long-range DIAL CO_2 measurement with the foothill target return measurement would be better for maintaining data quality.

6 Conclusions

The XCO_2 measurement from space requires a bias-free high precision of 1–2 ppm with a horizontal resolution of 100 km × 100 km. The IPDA lidar is one of candidate spaceborne sensors to measure the column-averaged mixing ratio of CO_2 using return signal from the Earth's surface. We need to discuss the detection sensitivity of a 2 µm IPDA lidar using a coherent detection and using a direct detection. In this paper, we used the coherent IPDA lidar with a 2 µm single-frequency Q-switched laser with laser frequency offset locking. Experimental horizontal CO_2 measurements were conducted using foothill target (trees and ground surface) and atmospheric (aerosol) returns in the western part of Tokyo

on 11, 27 and 28 December 2010. The CO_2 concentration was first measured with the 2 µm coherent IPDA lidar. The foothill target is located about 7.12 km south of NICT. The results obtained from the foothill target return were examined in detail and compared with those measured from the atmospheric return and the in situ sensor. The range measured using the 2 µm coherent IPDA lidar showed a large fluctuation related mainly to speckle-induced intensity fluctuation. The frequency distribution of the measured range showed the characteristics of mix reflection by the trees and the ground surface. For coherent lidar, it is difficult to measure the range with a high precision better than 1 m due to the long laser-pulse width. We derived a foothill target range with the precision of 0.012 km corresponding to the laser pulse width of 150 ns. Our results also indicated that the 2 µm coherent IPDA lidar has a potential for detecting the ground surface return from the backscattered signal. Though the PDF in negative exponential function can be expected if the signal is backscattered only from the ground surface, analyzed data showed the Nc = 1.9. The precisions of the 2 µm coherent IPDA lidar CO_2 measurement after the integration of 900, 4500 and 27000 shot pairs were 6.5, 2.8, and 1.2 %. As described by Ehret et al. (2008), the results also indicated that a laser operating at a high pulse repetition frequency of a few tens of KHz is necessary for the coherent IPDA lidar XCO_2 measurement at the target horizontal resolution of 100 km × 100 km from space. The averages values of the 2 µm coherent IPDA lidar measurements were about 5 ppm lower than the 5 min running averages of the in situ sensor, because of the spatial difference, the f1uctuation of temperature, and the natural variability of CO_2 along the observed line of sight. Statistical comparisons indicated that there were no bias between foothill target and atmospheric return measurements. We can obtain more stable data from the 2 µm coherent IPDA lidar. The CO_2 volume mixing ratio change of 3 % is detectable by the 2 µm coherent IPDA lidar if the signal is integrated during 5 min. The calibration of the on- and off-line return powers was carried out at a range of 0.974 km and the bias of the optical depth was negligible. In order to make accurate XO_2 measurements for the foothill target, it is important to make a precise range measurement using a Q-switched laser and a range-gated receiver. The IPDA lidar has a great advantage in terms of reducing uncertainty due to the presence of aerosols and clouds.

Acknowledgements. The authors would like to thank Robert T. Menzies and an anonymous reviewer for their helpful and valuable comments that helped to improve our paper essentially.

Edited by: G. Ehret

References

Abshire, J. B., Riris, H., Allan, G. R., Weaver, C. J., Mao, J., Sun, X., Hasselbrack, W. E., Kawa, S. R., and Biraud, S.: Pulsed airborne lidar measurement of atmospheric CO_2 column absorption, Tellus B, 52, 770–783, doi:10.1111/j.1600-0889.2010.00502.x, 2010.

Amediek, A., Fix, A., Wirth, M., and Ehret, G.: Development of an OPO system at 1.57 µm for integrated path DIAL measurement of atmospheric carbon dioxide, Appl. Phys. B, 92, 295–302, doi:10.1007/s00340-008-3075-6, 2008.

Browell, E. V., Dobler, J., Kooi, S. A., Choi, Y., Harrison, F. W., Moore III, B., and Zaccheo, T. S.: Airborne validation of laser remote measurements of atmospheric carbon dioxide, Proc. 25th Int. Laser Radar Conf., 1, S6O-03, 2010.

Crisp, D., Atlas, R. M., Breon, F.-M., Brown, L. R., Burrows, J. P., Ciais, P., Connor, B. J., Doney, S. C., Fung, I. Y., Jacob, D. J., Miller, C. E., O'Brien, D., Pawson, S., Randerson, J. T., Rayner, P., Salawitch, R. J., Sander, S. P., Sen, B., Stephens, G. L., Tans, P. P., Toon, G. C. Wennberg, P. O., Wofsy, S. C., Yung, Y. L., Kuang, Z., Chudasama, B., Sprague, G., Weiss, B., Pollock, R., Kenyon, D., and Schroll, S.: The Orbiting Carbon Observatory mission, Adv. Space. Res., 34, 700–709, 2004.

Ehret, G., Kiemle, C., Wirth, M., Amediek, A., Fix, A., and Houweling, S.: Space-borne remote sensing of CO_2, CH_4, and N_2O by integrated path differential absorption lidar: a sensitivity analysis, Appl. Phys. B, 90, 593–608, doi:10.1007/s00340-007-2892-3, 2008.

Etheridge, D. M., Steele, L. P., Langenfelds, R. L., Francey, R. J., Barnola, J.-M., and Morgan, V. I.: Natural and anthropogenic changes in atmospheric CO_2 over the last 1000 years from air in Antarctic ice and firn, J. Geophys. Res., 101, 4115–4128, 1996.

Frehlich, R., Hannon, S. M., and Henderson, S. W.: Coherent Doppler lidar measurements of winds in the weak signal regime, Appl. Optics, 36, 3491–3499, 1997.

Gibert, F., Flamant, P. H., Bruneau, D., and Loth, C.: Two-micrometer heterodyne differential absorption lidar measurements of the atmospheric CO_2 mixing ratio in the boundary layer, Appl. Optics, 45, 4448–4458, 2006.

Gibert, F., Flamant, P. H., Cuesta, J., and Bruneau, D.: Vertical 2 µm heterodyne differential absorption lidar measurements of mean CO_2 mixing ratio in the troposphere, J. Atmos. Ocean. Tech., 25, 1477–1499, 2008.

Goodman, J. W.: Statistical Optics, Wiley Classics Library, New York, 2000.

Intergovernmental Panel on Climate Change (IPCC), Climate change 2007: The Physical Science Basis: Contribution of Working Group I to the Fourth Assessment Report of the Intergovernmental Panel on Climate Change, edited by: Solomon, S., Qin, D., Manning, M., Chen, Z., Marquis, M., Averyt, K. B., Tignor, M., and Miller, H. L., Cambridge University Press, Cambridge, UK and New York, NY, USA, 996 pp., 2007.

Ishii, S., Mizutani, K., Fukuoka, H., Ishikawa, T., Philippe, B., Iwai, H., Aoki, T., Itabe, T., Sato, A., and Asai, K.: Coherent 2 µm differential absorption and wind lidar with conductively-cooled Laser and two-axis scanning device, Appl. Optics, 49, 1809–1817, 2010.

Ishii, S., Mizutani, K., Baron, P., Iwai, H., Oda, R., Itabe, T., Fukuoka, H., Ishikawa, T., Koyama, M., Tanaka, T., Morino, I., Uchino, O., Sato, A., and Asai, K.: Partial CO_2 Column-

averaged Dry-air Mixing Ratio from Measurements by coherent 2 µm differential absorption and wind lidar with Laser Frequency Offset Locking, J. Atmos. Ocean. Tech., 29, 1169–1181, doi:10.1175/JTECH-D-11-00180.1, 2012.

Kanda, M., Moriwaki, R., and Kimoto Y.: Temperature profiles within and above an urban canopy, Bound.-Lay. Meteorol., 115, 499–506, 2005.

Kawa, S. R., Mao, J., Abshire, J. B., Collatz, G. J., Sun, X., and Weaver, C. J.: Simulation studies for a space-based CO_2 lidar mission, Tellus B, 62, 759–769, 2010.

Koch, G. J., Barnes, B. W., Petros, M., Beyon, J. Y., Amzajerdian, F., Yu, J., Davis, R. E., Ismail, S., Vay, S., Kavaya, M. J., and Singh, U. N.: Coherent differential absorption lidar measurements of CO_2, Appl. Optics, 43, 5092–5099, 2004.

Koch, G., Beyon, J. Y., Gibert, F., Barnes, B. W., Ismail, S., Petros, M., Petzar, P. J., Yu, F. J., Modlin, E. A., Davis, K. J., and Singh, U. N.: Side-line tunable laser transmitter for differential absorption lidar measurements of CO_2: Design and application to atmospheric measurements, Appl. Optics, 47, 944–956, 2008.

Kuze, A., Suto, H., Nakajima, M., and Hamazaki, T.: Thermal and near infrared sensor for carbon observation Fourier-transform spectrometer on the Greenhouse Gases Observing Satellite for greenhouse gases monitoring, Appl. Optics, 48, 6716–6733, 2009.

Le Quéré, C., Raupach, M. R., Canadell, J. G., Marland, G., Marland, G., Bopp, L., Ciais, P., Conway, T. J., Doney, S. C., Feely, R. A., Foster, P., Friedlingstein, P., Gurney, K., Houghton, R. A., House, J. I., Huntingford, C., Levy, P. E., Lomas, M. R., Majkut, J., Metzl, N., Ometto, J. P., Peters, G. P., Prentice, I. C., Randerson, J. T., Running, S. W., Sarmiento, J. L., Schuster, U., Sitch, S., Takahashi, T., Viovy, N., Van Der Werf, G. R., Woodward, F. I.: Trends in the sources and sinks of carbon dioxide, Nat. Geosci., 2, 831–836, doi:10.1038/ngeo689, 2009.

Menzies, R. T. and Tratt, D. M.: Differential laser absorption spectrometry for global profiling of tropospheric carbon dioxide: selection of optimum sounding frequencies for high-precision measurements, Appl. Optics, 42, 6569–6577, 2003.

NASA Science Definition and Planning Workshop Report: Active Sensing of CO_2 Emissions over Nights, Days, and Seasons (ASCENDS), available at: http://decadal.gsfc.nasa.gov/documents/12-30-08-ASCENDS_Workshop.pdf (last access: 22 May 2013), 2008.

Rye, B. J. and Hardesty, R. M.: Estimate optimization parameters for incoherent backscatter heterodyne lidar, Appl. Optics, 36, 9425–9436, 1997.

Sakaizawa, D., Kawakami, S., Nakajima, M., Sawa, Y., and Matsueda, H.: Ground-based demonstration of CO_2 remote sensor using 1.57 µm differential laser absorption spectrometer with direct detection, J. Appl. Remote. Sens., 4, 043548, doi:10.1117/1.3507092, 2010.

Sato, A, Miyake, Y., Asai, K., Ishii, S., and Mizutani, K.: Tunable, Q-switched Tm,Ho:LLF laser with a conductively cooled triangular prism rod, Appl. Optics, 51, 1236–1240, 2012.

Spiers, G. D., Menzies, R. T., Jacob, J., Christensen, L. E., Phillips, M. W., Choi, Y., and Browell, E. V.: Atmospheric CO_2 measurements with a 2 µm airborne laser absorption spectrometer employing coherent detection, Appl. Optics, 50, 2098–2111, 2011.

Yu, J., Trieu, B. C., Petros, M., Bai, Y., Petzar, P. J., Koch, G. J., Singh, U. N., and Kavaya, M. J.: Advanced 2-µm solid-state laser for wind and CO_2 lidar applications, Society of Photo-Optical Instrumentation Engineers (SPIE) Conference Series, edited by: Singh, U. N., Vol. 5575 of Society of Photo-Optical Instrumentation Engineers (SPIE) Conference Series, 6409, C4091–C4091, doi:10.1117/12.696908, 2006.